BIOLOGICAL CRYSTALLOGRAPHY

ISSN 1399-0047

The mechanism of substrate-controlled allosteric regulation of SAMHD1 activated by GTP

Chun-Feng Zhu,[a]‡ Wei Wei,[a,b,c]‡ Xin Peng,[a] Yu-Hui Dong,[b] Yong Gong[b]* and Xiao-Fang Yu[a,c,d,e]*

[a]School of Life Sciences, Tianjin University, Tianjin, People's Republic of China, [b]Beijing Synchrotron Radiation Facility, Institute of High Energy Physics, Chinese Academy of Sciences, 19B Yuquan Road, Shijingshan District, Beijing 100049, People's Republic of China, [c]Institute of Virology and AIDS Research, First Hospital of Jilin University, Changchun, Jilin Province, People's Republic of China, [d]Department of Molecular Microbiology and Immunology, Johns Hopkins Bloomberg School of Public Health, Baltimore, Maryland, USA, and [e]Collaborative Innovation Center of Chemical Science and Engineering, Tianjin, People's Republic of China. *Correspondence e-mail: yonggong@ihep.ac.cn, xfyu@tju.edu.cn

Received 3 October 2014
Accepted 17 December 2014

‡ These authors contributed equally.

Keywords: SAMHD1; substrate-controlled allosteric regulation.

PDB references: SAMHD1, complex with GTP, 4rxo; complex with GTP and dATP, 4rxp; complex with GTP and dUTP, 4rxq; complex with GTP and dCTP, 4rxr; complex with GTP and dTTP, 4rxs

Supporting information: this article has supporting information at journals.iucr.org/d

SAMHD1 is the only known eukaryotic deoxynucleoside triphosphate triphosphohydrolase (dNTPase) and is a major regulator of intracellular dNTP pools. It has been reported to be a potent inhibitor of retroviruses such as HIV-1 and endogenous retrotransposons. Previous crystal structures have revealed that SAMHD1 is activated by dGTP-dependent tetramer formation. However, recent data have indicated that the primary activator of SAMHD1 is GTP, not dGTP. Therefore, how its dNTPase activity is regulated needs to be further clarified. Here, five crystal structures of the catalytic core of SAMHD1 in complex with different combinations of GTP and dNTPs are reported, including a GTP-bound dimer and four GTP/dNTP-bound tetramers. The data show that human SAMHD1 contains two unique activator-binding sites in the allosteric pocket. The primary activator GTP binds to one site and the substrate dNTP (dATP, dCTP, dUTP or dTTP) occupies the other. Consequently, both GTP and dNTP are required for tetramer activation of the enzyme. In the absence of substrate binding, SAMHD1 adopts an inactive dimer conformation even when complexed with GTP. Furthermore, SAMHD1 activation is regulated by the concentration of dNTP. Thus, the level of dNTP pools is elegantly regulated by the self-sensing ability of SAMHD1 through a novel activation mechanism.

1. Introduction

Deoxynucleoside triphosphates (dNTPs) are essential for DNA replication and other diverse biological processes. The maintenance of optimal intracellular concentrations of dNTPs is critical for the survival of all organisms. SAM domain and HD domain-containing protein 1 (SAMHD1) is the only known eukaryotic deoxynucleoside triphosphate triphosphohydrolase (dNTPase; Powell *et al.*, 2011; Goldstone *et al.*, 2011) and is a major regulator of intracellular dNTP pools (Franzolin *et al.*, 2013). Human mutations in SAMHD1 have been linked to cancer (Clifford *et al.*, 2014; Landau *et al.*, 2013) and the autoimmune disease Aicardi–Goutières syndrome (Rice *et al.*, 2009).

Recently, SAMHD1 has been reported to be a potent inhibitor of retroviruses such as HIV-1 (Laguette *et al.*, 2011; Hrecka *et al.*, 2011; Berger *et al.*, 2011; Roesch & Schwartz, 2013; Descours *et al.*, 2012; Baldauf *et al.*, 2012), DNA viruses (Hollenbaugh *et al.*, 2013; Kim *et al.*, 2013) and endogenous retrotransposons (Zhao *et al.*, 2013). The dNTPase activity of SAMHD1 creates a low dNTP concentration status in myeloid

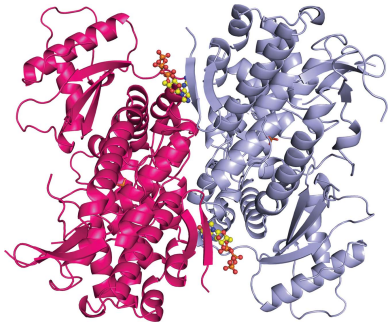

cells (Lahouassa *et al.*, 2012) and resting CD4 T+ cells (Baldauf *et al.*, 2012), thereby inhibiting the reverse transcription of diverse retroviruses. The virion-associated Vpx protein (Henderson *et al.*, 1988; Yu *et al.*, 1988, 1991; Accola *et al.*, 1999; Selig *et al.*, 1999; Paxton *et al.*, 1993; Wu *et al.*, 1994) of HIV-2 and certain SIV strains neutralizes the antiviral activity of SAMHD1 by promoting its proteasome-dependent degradation (Hrecka *et al.*, 2011; Laguette *et al.*, 2011). Vpx binds DCAF1 using conserved motifs in helix 1 and helix 3, which in turn recruit other components of the CRL4 (DCAF1) E3 ubiquitin ligase (Ahn *et al.*, 2012; Ayinde *et al.*, 2012; Berger *et al.*, 2012; Brandariz-Nuñez *et al.*, 2012; Hofmann *et al.*, 2012; Lahouassa *et al.*, 2012; Wei *et al.*, 2012; Schwefel *et al.*, 2014) to facilitate SAMHD1 ubiquitination and subsequent degradation. Resting CD4+ T cells and monocytes are resistant to retroviral infection because of their low dNTP concentrations. However, a critical concentration of dNTPs is still required for mitochondrial DNA replication and DNA repair in these resting cells.

The dNTPase activity of SAMHD1 can be activated by dGTP as a tetramer (Zhu *et al.*, 2013; Yan *et al.*, 2013; Ji *et al.*, 2013). Our previous crystal structure revealed homotetrameric SAMHD1 in complex with the allosteric activator dGTP and the substrate dGTP/dATP (Zhu *et al.*, 2013). Nevertheless, the primary activator of SAMHD1 dNTPase activity is GTP, which is 1000-fold more abundant than dGTP (Amie *et al.*, 2013; Gavegnano *et al.*, 2012; Hansen *et al.*, 2014). Since GTP cannot be hydrolyzed by SAMHD1, how SAMHD1 dNTPase activity is regulated (and therefore not constitutively activated in the presence of GTP) in order to maintain optimal intracellular concentrations of dNTPs is not clear.

In this study, to understand the structural basis for the co-activation of SAMHD1 by GTP and substrates, we have determined the mechanism of SAMHD1 dNTPase regulation by GTP using both structural and functional approaches. Five crystal structures of the SAMHD1 catalytic core (109–626) in complex with GTP, GTP/dATP, GTP/dCTP, GTP/dUTP and GTP/dTTP were solved.

2. Materials and methods

2.1. Plasmid construction

DNA encoding residues 109–626 of human SAMHD1, which is the catalytic core, was generated by PCR with primers containing BamHI and SalI cleavage sites (SAMHD1 109–626F, 5′-GGATCCCAAATCCACGTTGATACAATGAA-3′; SAMHD1 109–626R, 5′-GTCGACTCACATTGGGTCATCTT-3′). The PCR products were cloned into the pET-28a-Plus vector with a His_6 tag at the N-terminus.

2.2. Recombinant protein expression and purification

For expression, the SAMHD1 expression vector was transformed into *Escherichia coli* BL21(DE3) cells. The protein was overexpressed overnight at 16°C by induction with 0.1 m*M* isopropyl *β*-D-1-thiogalactopyranoside (IPTG). Harvested cells were lysed in 20 m*M* Tris–HCl pH 8.0, 150 m*M* NaCl and then clarified by sonication and centrifugation at 13 000*g* for 30 min. The expressed proteins were purified by metal-affinity chromatography on chelation resin and size-exclusion chromatography on a Superdex 200 10/300 GL column. To determine the effect of various substrates on the formation of the tetramer when GTP is the activator, purified recombinant SAMHD was exchanged into buffer consisting of 20 m*M* Tris–HCl pH 8.0, 200 m*M* NaCl, 5 m*M* $MgCl_2$, 5 m*M* DTT. Various substrates (dATP, dUTP, dCTP and dTTP) were added to a final concentration of 25 m*M* each. The mixtures were incubated at 4°C for 2 h and were then analyzed by size-exclusion chromatography.

2.3. Size-exclusion chromatography

Each SAMHD1 complex was concentrated to <500 µl and loaded onto a Superdex 200 10/300 GL column (GE Healthcare) with a 500 µl loop and run at a flow rate of 0.3 ml min^{-1}; the column was calibrated using vitamin B_{12} (1370 Da), myoglobin (17 000 Da), ovalbumin (44 000 Da), *γ*-globulin (158 000 Da) and thyroglobulin (670 000 Da) as standards. The gel-filtration buffer for SAMHD1 was composed of 20 m*M* Tris–HCl pH 8.0, 150 m*M* NaCl, 5 m*M* $MgCl_2$.

2.4. Protein crystallization and X-ray data collection

For crystallization, the SAMHD1 protein was concentrated to 7.5 mg ml^{-1} with 20 m*M* Tris–HCl buffer containing 5 m*M* $MgCl_2$, 0.2 *M* NaCl, 0.5 m*M* tris-(2-carboxyethyl)phosphine (TCEP); 300–500 µ*M* GTP was added to the buffer used to obtain crystals of the GTP-bound dimer and 100 µ*M* GTP and 25 m*M* different dNTPs were added to the buffers used to obtain crystals of the GTP/dNTP-bound tetramers. Crystals were grown at 22°C using the sitting-drop vapour-diffusion method. Crystallization was performed under conditions from commercially available crystallization screening kits. Crystals of the GTP-bound dimer were grown in 0.2 *M* sodium chloride, 0.1 *M* sodium/potassium phosphate, 25%(*w*/*v*) polyethylene glycol 1000 pH 6.5. Crystals of the GTP/dNTP-bound tetramers were grown in 0.1 *M* lithium sulfate monohydrate, 0.1 *M* sodium citrate tribasic dihydrate, 20%(*w*/*v*) polyethylene glycol 1000 pH 5.5. Diffraction data were collected on the 1W2B beamline at the Institute of High Energy Physics, the BL17U beamline at Shanghai Synchrotron Radiation Facility and the BL1A beamline at Photon Factory, Japan and were processed with *HKL*-2000 (Otwinowski & Minor, 1997). The structures of the GTP-bound dimer and the GTP/dNTP-bound tetramers were determined by molecular replacement using *Phaser* (Vagin & Teplyakov, 2010) from the *CCP*4 program suite (Winn *et al.*, 2011). PDB entries 3u1n (Goldstone *et al.*, 2011) and 4mz7 (Zhu *et al.*, 2013) were used as the initial search models. Structure refinement was performed with *REFMAC* (Murshudov *et al.*, 2011) and *PHENIX* (Adams *et al.*, 2010) and model building was performed with *Coot* (Emsley & Cowtan, 2004). The quality of the final structures was evaluated using *PROCHECK* (Laskowski *et al.*, 1993). The Ramachandran plots showed that >98% of the residues were in the most favoured region. The details of data

Table 1
Data-collection and refinement statistics.

Values in parentheses are for the highest resolution shell.

	SAMHD1–GTP dimer	SAMHD1–GTP–dATP tetramer	SAMHD1–GTP–dUTP tetramer	SAMHD1–GTP–dCTP tetramer	SAMHD1–GTP–dTTP tetramer
Data collection					
Space group	$P2_1$	$C2$	$C2$	$C2$	$C2$
Unit-cell parameters					
a (Å)	77.2	151.2	150.8	150.9	151.7
b (Å)	183.2	108.1	108.9	108.3	109.8
c (Å)	81.3	92.4	92.2	92.7	93.0
α (°)	90.0	90.0	90.0	90.0	90.0
β (°)	100.6	123.0	122.7	123.0	122.8
γ (°)	90.0	90.0	90.0	90.0	90.0
Wavelength (Å)	1.10	0.98	0.98	0.98	1.10
Resolution (Å)	50–2.6 (2.64–2.60)	50–2.1 (2.14–2.10)	50–2.1 (2.14–2.10)	50–2.1 (2.14–2.10)	50–2.2 (2.24–2.20)
$R_{\rm merge}$†	0.083 (0.570)	0.078 (0.591)	0.073 (0.713)	0.075 (0.576)	0.065 (0.637)
$\langle I/\sigma(I)\rangle$	13.2 (1.7)	40.3 (6.0)	46.1 (6.9)	39.4 (3.9)	19.1 (1.7)
Completeness (%)	96.8 (93.0)	99.9 (100.0)	99.9 (100.0)	99.6 (99.1)	100.0 (100.0)
Average multiplicity	5.9	6.7	7.2	6.9	6.8
Overall B factor from Wilson plot (Å^2)	55.3	33.1	35.2	43.0	40.0
Refinement					
Resolution (Å)	50–2.60	50–2.10	50–2.10	50–2.10	50–2.20
No. of reflections	62523	68880	69319	66701	61677
$R_{\rm work}/R_{\rm free}$‡	0.183/0.222	0.180/0.208	0.197/0.229	0.175/0.213	0.194/0.222
No. of atoms					
Protein	14493	7972	7972	7972	7883
Ligands	148	184	176	176	180
Ions	4	2	2	2	2
Water	332	492	518	428	407
Average B factor (Å^2)	65.7	38.6	41.1	49.7	50.5
R.m.s. deviations§					
Bond lengths (Å)	0.008	0.008	0.009	0.008	0.008
Bond angles (°)	1.3	1.3	1.3	1.3	1.3
Ramachandran statistics, residues in¶ (%)					
Most favoured regions	98.8	98.9	98.2	98.7	98.0
Allowed regions	1.8	1.1	1.8	1.3	2.0
Disallowed regions	0	0	0	0	0

† $R_{\rm merge} = \sum_{hkl}\sum_i |I_i(hkl) - \langle I(hkl)\rangle| / \sum_{hkl}\sum_i I_i(hkl)$, where hkl indicates unique reflection indices and i indicates symmetry-equivalent indices. ‡ $R_{\rm work} = \sum_{hkl} ||F_{\rm obs}| - |F_{\rm calc}|| / \sum_{hkl} |F_{\rm obs}|$, where $|F_{\rm obs}|$ and $|F_{\rm calc}|$ are the observed and calculated structure-factor amplitudes, respectively. $R_{\rm free}$ is calculated using 5% of the reflections, which were randomly excluded from refinement. § Ideal values as defined by Engh & Huber (1991). ¶ The Ramachandran statistics were calculated using *PROCHECK* (Laskowski *et al.*, 1993).

collection and structure refinement are presented in Table 1. All figures were prepared with *PyMOL* (http://www.pymol.org).

2.5. dNTPase activity assays

dNTPase assays were carried out in a reaction buffer consisting of 20 m*M* Tris–HCl pH 7.8, 50 m*M* NaCl, 5 m*M* $MgCl_2$, the appropriate dNTPs (each at 0.5 m*M*) and 0.8 m*M* protein at 25°C. The reactions were initialized and subsequently terminated by the addition of the enzyme and of 0.5 *M* EDTA to a final concentration of 10 m*M*, respectively. A final volume of 250 ml was used for all reactions. Aliquots collected at various time points were centrifuged using an Amicon Ultra 0.5 ml 10 kDa filter (Millipore) at 12 000*g* for 20 min. Deproteinized samples were analyzed with a Waters HPLC system using a 150 × 4.6 mm C18 column (Agela Technologies). The column was equilibrated at 40°C in 10 m*M* triethylamine in water at pH 5.0 (buffer *A*). Injected samples were eluted with a 5 min isocratic buffer phase followed by a methanol gradient over 30 min at a flow rate of 0.2 ml min^{-1}. The absorbance at 260 nm was used to detect the eluted compounds in all cases.

3. Results

3.1. GTP and substrate are required for SAMHD1 tetramer formation

Tetramer formation is a prerequisite for SAMHD1 dNTPase activity (Zhu *et al.*, 2013; Yan *et al.*, 2013; Ji *et al.*, 2013). Although GTP is the primary activator of the dNTPase activity of SAMHD1, GTP alone was unable to activate SAMHD1 to induce SAMHD1 tetramer formation, but it did induce dimer formation (Supplementary Fig. S1). As expected, the substrate alone (dATP) did not induce SAMHD1 tetramer formation (Supplementary Fig. S1*a*). Only when both GTP and dATP were present was SAMHD1 tetramer formation detected. Other dNTP substrates, such as dCTP (Supplementary Fig. S1*b*) and dTTP (Supplementary Fig. S1*c*), as well as the noncanonical dUTP (Supplementary Fig. S1*d*), also induced formation of the SAMHD1 tetramer when mixed with GTP.

3.2. Crystal structure of the GTP-bound SAMHD1 dimer

We determined the crystal structure of the human SAMHD1 catalytic core (residues 109–626) with GTP alone at

2.6 Å resolution in space group $P2_1$. The overall structure shows a dimeric form (Fig. 1*a*) with a 1:1 stoichiometry of SAMHD1 and GTP. Only one GTP was detected per SAMHD1 molecule, and it bound to each allosteric site between two monomers (Fig. 1*b*). Density for GTP was observed and unambiguously defined in the electron-density map (Fig. 1*c*). As shown in Fig. 1(*d*), GTP interacts with Arg451 from one chain of the SAMHD1 dimer and Lys116, Val117, Asp137, Gln142 and Arg145 from the other.

The N-terminal region of the GTP-bound dimer consists of two β-sheets (β1 and β2), whereas the same region has been found to be a disordered loop in the crystal structure of the SAMHD1 catalytic core dimer in the absence of GTP (PDB entry 3u1n; Goldstone *et al.*, 2011). Comparison of the GTP-bound dimer with the dimer in the absence of GTP revealed that the N-terminal β-sheets are a key basis for the binding of GTP at the allosteric site (Fig. 2*a*). Moreover, we were able to construct a more complete C-terminal region in the GTP-bound dimer, as shown in Fig. 2(*b*). The region containing amino acids 502–510, which was not traced in PDB entry 3u1n, was found to block the active pocket of SAMHD1, as shown in Supplementary Fig. S2.

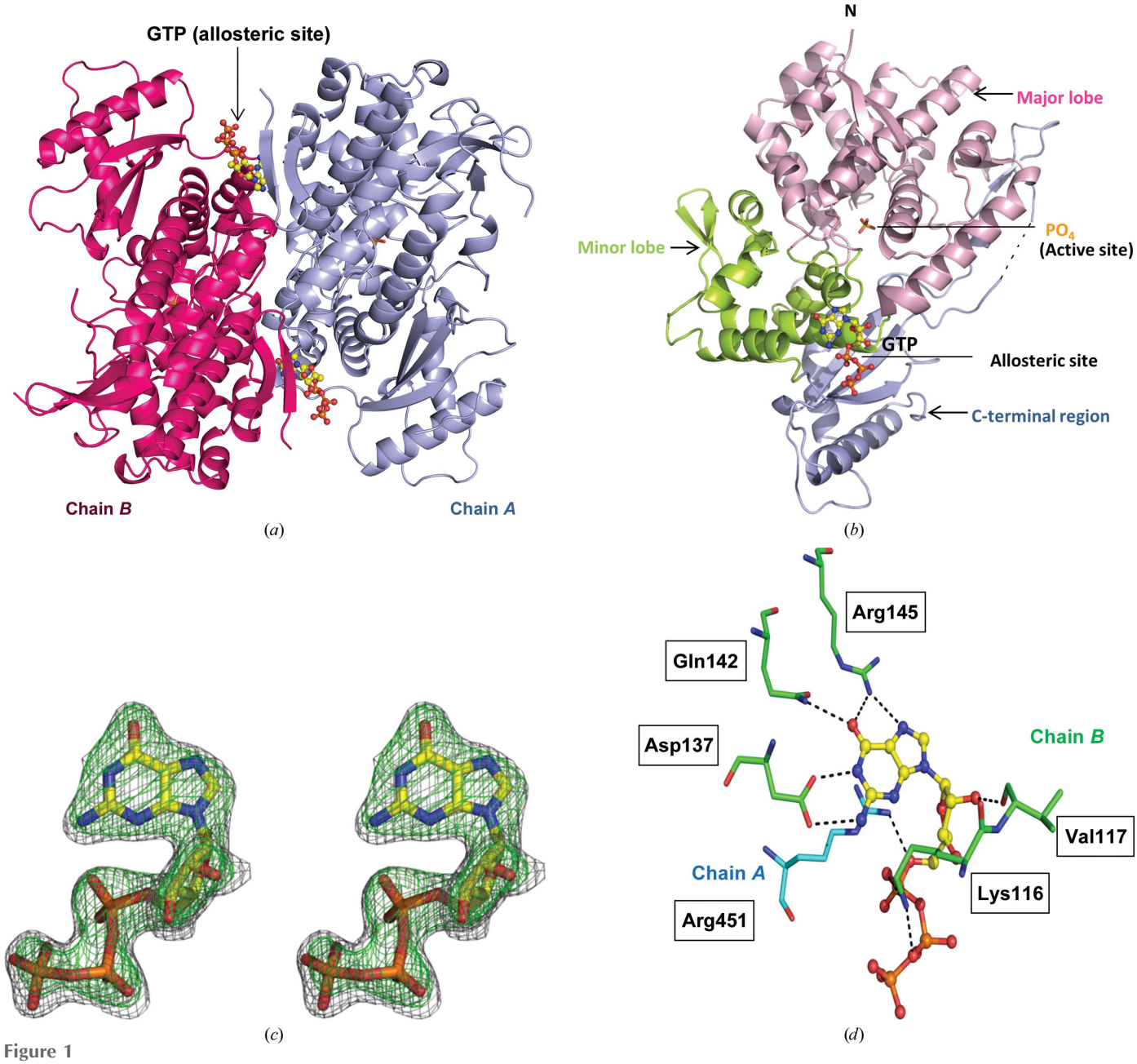

Figure 1
Crystal structure of the GTP-bound SAMHD1 dimer. (*a*) Architecture of the SAMHD1 dimer shown as a ribbon representation. A primary activator GTP at the dimer interface is indicated by an arrow. (*b*) Representation of the SAMHD1 monomer from the GTP-bound SAMHD1 dimer showing the major lobe, minor lobe and C-terminal region. GTP is shown in ball-and-stick representation. (*c*) A stereo image of the electron-density map for GTP in the allosteric site. A $2F_o - F_c$ GTP-omitted electron-density map (grey, contoured at 1σ) and a $F_o - F_c$ map (green, contoured at 3σ) are shown. (*d*) Detailed interactions in the allosteric pocket of the SAMHD1 dimer. Chain *A*, blue; chain *B*, green.

3.3. Crystal structure of GTP/dNTP-bound SAMHD1 tetramers

We determined four crystal structures of the human SAMHD1 catalytic core (residues 109–626) with GTP plus different substrates (dATP, dCTP, dUTP and dTTP) at 2.1–2.2 Å resolution. Each of them consisted of a tetramer and belonged to space group *C*2 (Fig. 3*a*). The asymmetric unit contains a homodimer related by a crystallographic twofold axis to form a tetrameric assembly with approximate 222 symmetry. One GTP and one dNTP were detected in each allosteric site of the SAMHD1 tetramer with an extensive network of interactions (Fig. 3*b*), and one dNTP molecule was found in each active site. In the allosteric sites, the densities of the different dNTPs were unambiguously defined in the electron-density map, as shown in Fig. 3(*c*).

3.4. Structural basis for the selective binding of nucleotides at the allosteric sites of SAMHD1

Examination of the different nucleotide-bound SAMHD1 structures indicated that SAMHD1 contains two unique activator-binding sites in the allosteric pocket of the active tetramer. The primary activator GTP binds to one site (the G site) and the dNTP substrate occupies the other (the S site). The GTP-binding site (G site) has a preference for GTP because of a specific amino-acid interaction with the guanine base (Fig. 3*b*). At the G site, Asp137 forms a strong hydrogen bond to the amino N2 atom of GTP or dGTP. This interaction should be missing when ATP (or dATP) is present at this site, since Arg451 interacts with GTP but presumably not with ATP or dATP. The 2′ OH of the GTP sugar forms a hydrogen bond to Val117 (which is missing in the dGTP complex; Fig. 3*b*). Although dGTP could also be tolerated at the G site, it is unlikely to occur in the cell because of the prohibitively (1000-fold) higher concentration of GTP compared with dGTP (Gavegnano *et al.*, 2012), while the other dNTPs and NTPs are disfavoured because of poor interactions with the surrounding amino acids at the G site.

The second site in the allosteric pocket can only tolerate dNTP as a substrate (S site) and not GTP or another NTP because of steric hindrance of the O atom of the NTP molecules by Phe157 (Fig. 4). The Phe157 benzyl group also forms a hydrophobic interaction with the benzyl group of dNTP. We also observed interactions between dNTP and other surrounding amino acids at the S site (Fig. 3*b*). All of the head groups of the substrates dATP, dCTP, dUTP and dTTP interact with the side chain of Asn119 of SAMHD1 through hydrogen bonds (Fig. 3*c*). Val156 and Arg333 of SAMHD1 bind to the deoxyribose sugars of the substrates, and mutations of these residues reduce or abolish the dNTPase activity (Supplementary Fig. S3). Thus, substrate binding at the allosteric site is critical for the dNTPase activity of SAMHD1.

The detailed interactions in the allosteric pocket of the SAMHD1 dimer (Fig. 1*d*) and tetramer (Fig. 3*b*) reveal the mechanism of tetramer formation. In the GTP-bound SAMHD1 dimer, GTP binding is coordinated by two protein chains. In contrast, in the GTP/dNTP-bound SAMHD1 tetramer three separate protein chains are involved in GTP and dNTP binding. The binding of the third chain is almost exclusively mediated by dNTP. Thus, binding of substrate (such as dATP) to the S site is a prerequisite for two dimers to form a tetramer. Consequently, GTP can only induce dimer formation, whereas GTP and dNTP trigger tetramer formation and conformational changes in SAMHD1.

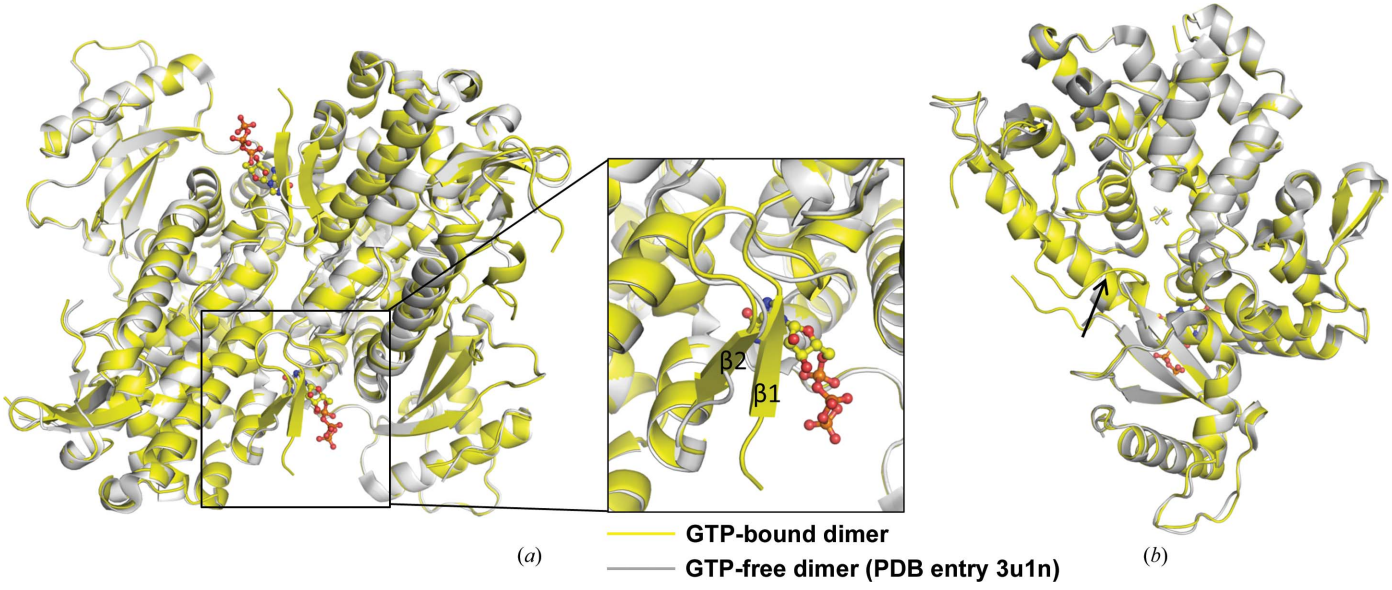

Figure 2
Structural comparison of the GTP-bound SAMHD1 dimer (yellow) and the dimer in the absence of GTP (PDB entry 3u1n, grey). (*a*) Comparison of the two dimers. A locally enlarged view of the N-terminal regions with different conformations is shown on the right. GTP is shown in a ball-and-stick representation. (*b*) Comparison of the monomers. The region containing amino acids 502–510, which was one of the regions that was not traced in the GTP-free dimer, is indicated by an arrow.

3.5. Comparison of the GTP-bound dimer and the GTP/dNTP-bound tetramers reveals substrate-induced SAMHD1 conformational changes

To understand the structural basis for the co-activation of SAMHD1 by GTP and substrates, we compared the crystal structure of SAMHD1 in complex with GTP alone with those with GTP and dNTP. They share similar structures of the major lobes and minor lobes. However, GTP/dNTP-induced tetramerization induces a large conformational change in the SAMHD1 C-terminal region when compared with the GTP-induced dimer (Fig. 5). Meanwhile, the catalytic site of the GTP-bound SAMHD1 dimer is blocked by the C-terminal region, preventing substrate entry (Figs. 6*a* and 6*b*). In the presence of GTP and substrate, the C-terminal region moves away from the catalytic site of the activated SAMHD1 tetramer, allowing the substrate to enter the catalytic site (Figs. 6*a* and 6*c*). Furthermore, proper alignment of the substrate in the catalytic site is triggered by GTP and dNTP binding within the allosteric site, explaining why the tetramer is a more active dNTPase than the dimer.

3.6. Activation of the SAMHD1 tetramer depends on the dNTP concentration

The fact that GTP alone is not sufficient for tetramer formation suggests that the dNTPase activity of SAMHD1 can be regulated by the concentration of substrate dNTPs. Indeed, we observed that formation of the tetramer is dependent on the dATP concentration (Supplementary Fig. S4*a*). SAMHD1 tetramers were not detected in the presence of GTP alone or of GTP plus low concentrations of dATP. In contrast, SAMHD1 tetramers were detected in the presence of GTP plus high concentrations of dATP. Similar results were observed for the substrates dCTP (Supplementary Fig. S4*b*) and dTTP (Supplementary Fig. S4*c*). Thus, SAMHD1 dNTPase activity is not constitutively activated because GTP cannot activate SAMHD1 alone, and its activity is further regulated by the concentration of dNTPs. SAMHD1 could serve as a major intracellular sensor of dNTP and maintain optimum levels of dNTPs that are sufficient for DNA repair and mitochondrial DNA replication but that restrict retroviral DNA synthesis.

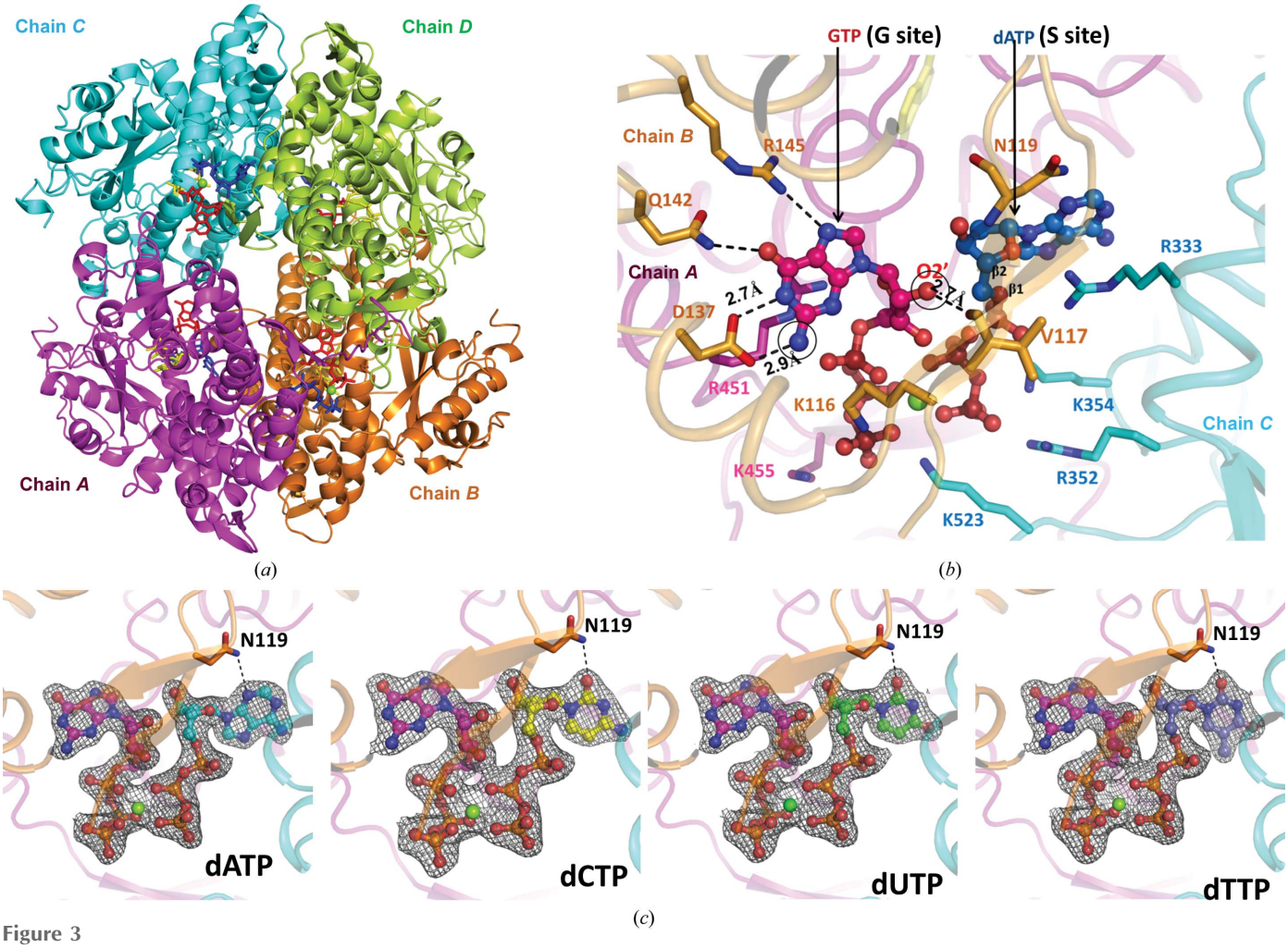

Figure 3
Crystal structure of the GTP/dNTP-bound SAMHD1 tetramer. (*a*) Architecture of the SAMHD1 tetramer shown as a ribbon representation. The substrate at the catalytic site (yellow), GTP activator (red) and dATP (blue) at the allosteric site are shown as sticks. Mg^{2+} ions (green) are shown as spheres. (*b*) Detailed view of the interactions in the allosteric site of the tetramer. The residues that bind GTP/dNTP directly are shown as sticks. (*c*) $2F_o - F_c$ electron-density maps (grey, contoured at 1σ) for different substrates (dATP, dCTP, dUTP and dTTP) in the allosteric site.

4. Discussion

Using structural and functional approaches, we have now determined the mechanism of dNTPase regulation by SAMHD1. We first demonstrated that GTP alone cannot activate the dNTPase activity of SAMHD1. The crystal structure of SAMHD1 complexed with GTP revealed an inactive catalytic dimer. Both GTP and substrates (dNTPs) are required to activate SAMHD1 to form tetramers. To understand the role of dNTPs in SAMHD1 activation, we also obtained crystal structures of GTP and substrate co-activated SAMHD1 tetramers. One of the most significant structural changes observed on activation was movement of the C-terminal region of the tetramer when compared with the inactive dimer. The C-terminal region of the dimer blocks the catalytic site, preventing substrate entry (Fig. 6). During tetramer formation, the C-terminal region moves away from the catalytic site, allowing the substrate to enter and the enzymatic reaction to occur.

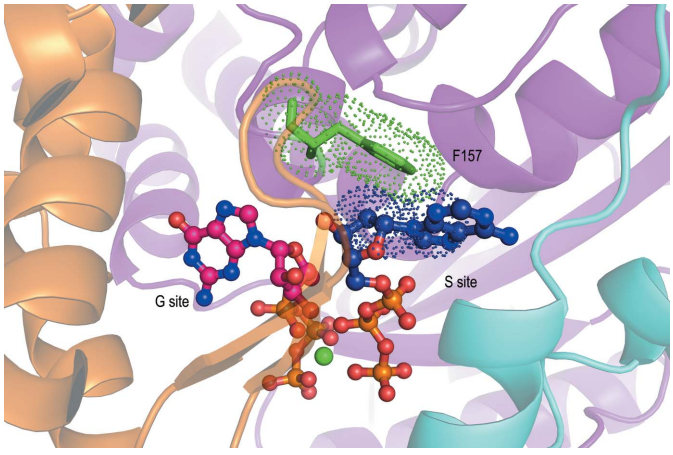

Figure 4
Repulsion of GTP at the S site. The benzyl group of Phe157 forms hydrophobic interactions with the head group of dNTP (represented as dots). The extra O2 in GTP will be disfavoured and excluded from the S site.

Our structures demonstrate that SAMHD1 contains two unique activator-binding sites in the allosteric pocket of the active tetramer. The primary activator GTP binds to one site (the G site) and the substrate dNTP occupies the other (the S site). Consequently, both GTP and dNTP are required for enzyme activation. Specific amino acids in the G site, such as Asp137 and Arg145, form unique interactions with GTP but not with the other NTPs, making GTP the primary activator of SAMHD1. On the other hand, GTP cannot enter the S site because of steric hindrance provided by Phe157. This situation allows the S site to serve as a unique sensor of dNTPs.

Guided by this structural information, we further demonstrated that substrate binding in the allosteric pocket is essential for hydrolase activity. More importantly, SAMHD1 activation is strictly dependent on dNTP concentrations. Thus, the levels of intracellular dNTP pools are elegantly regulated by the self-sensing ability of SAMHD1, and a model for the activation of SAMHD1 dNTPase activity is proposed (Fig. 7).

We would like to further point out that while a recent study reported the crystal structures of GTP/dNTP-bound tetramers (Ji *et al.*, 2014), we now also report the crystal structure of the GTP-bound inactive dimer for the first time. Furthermore, we provide the first report of a SAMDH1 structure (the GTP/dUTP tetramer) containing a noncanonical substrate as an activator.

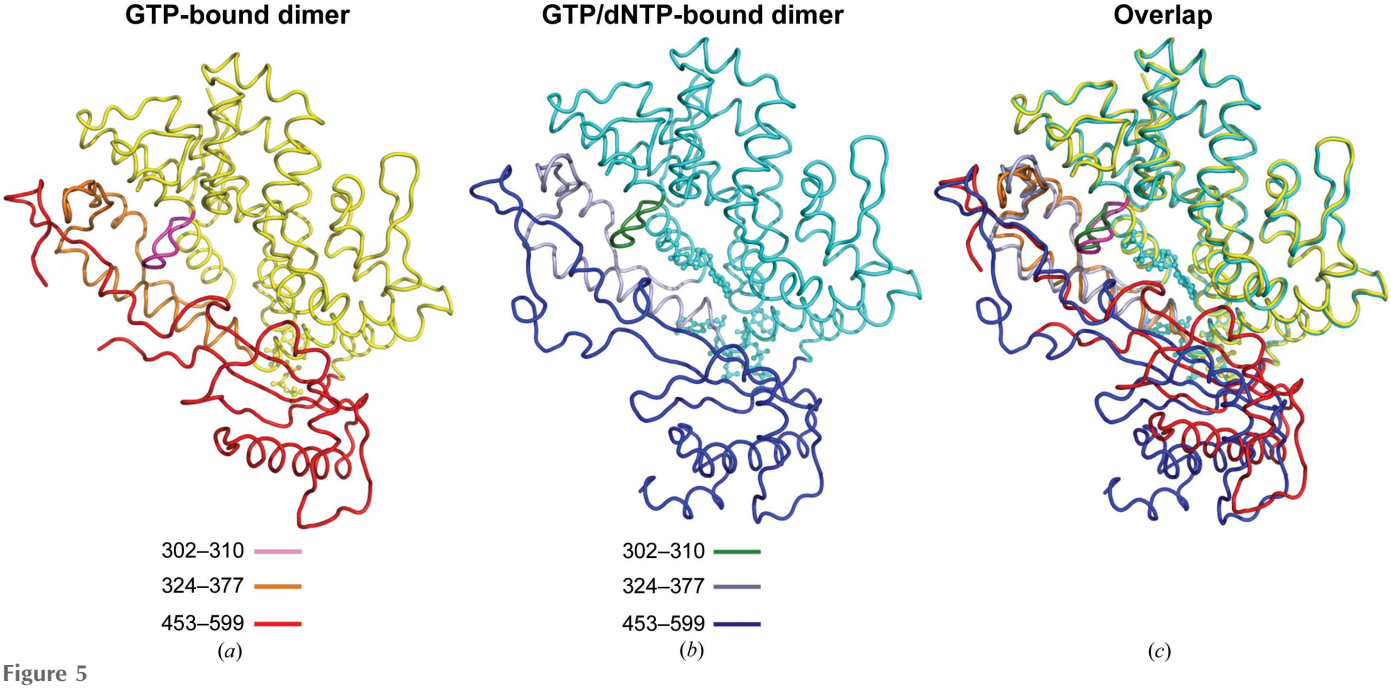

Figure 5
Comparison of the GTP-bound SAMHD1 dimer and the GTP/dNTP-bound SAMHD1 tetramer. (*a*) The GTP-bound SAMHD1 dimer. (*b*) The GTP/dNTP-bound SAMHD1 tetramer. (*c*) A comparison of the two structures. The regions with majorly differing conformations are highlighted in different colours and labelled.

Through a detailed comparison of the GTP-bound dimer and GTP/dNTP-bound tetramers, we have uncovered a novel and unique mechanism of SAMHD1 regulation by GTP. In contrast to previous reports, which have argued that the tetramerization alters the catalytic pocket from open to tight in order to fit the substrates (Ji *et al.*, 2013), the additional structural information available in our study reveals the conformational change at the catalytic pocket to be from closed to open.

In summary, our structural and functional studies shed light on the fundamental problem of dNTP regulation in cellular and molecular biology. The important role of SAMHD1 as a dNTP sensor explains the important balance between virus restriction and cellular survival as a result of elegant regulation by SAMHD1. Deregulation of dNTP levels as a result of SAMHD1 dysfunction may result in abnormal cell proliferation (tumours) and improper DNA damage response (autoimmune disease). Indeed, we have observed that SAMHD1

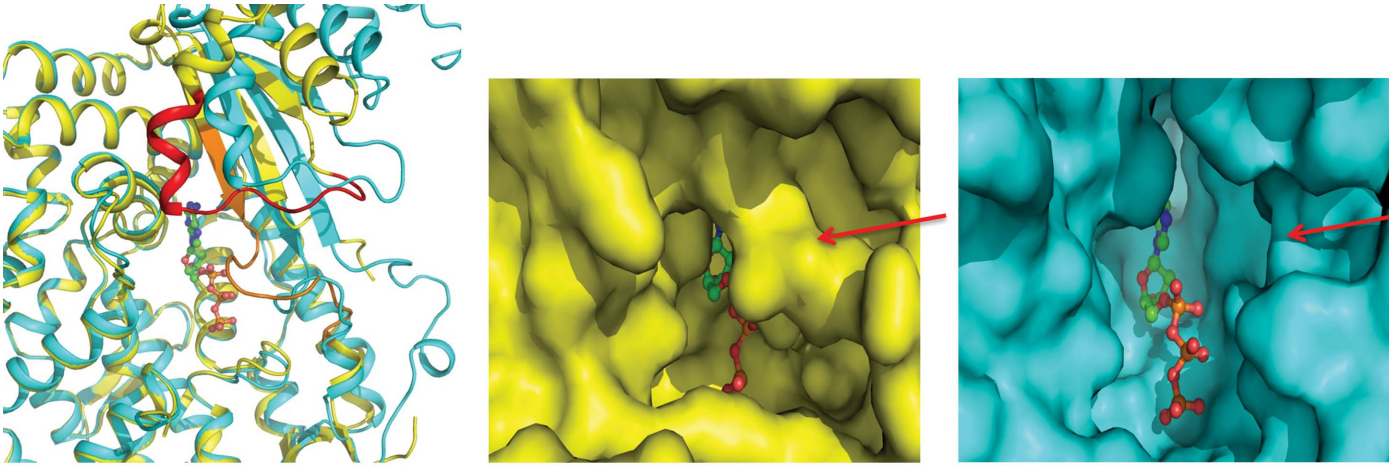

Figure 6
Detailed comparison of the catalytic sites of the SAMHD1 dimer and tetramer. (*a*) The catalytic sites of the GTP/dATP-bound SAMHD1 tetramer (blue) and the GTP-bound SAMHD1 dimer (yellow) are overlaid. Amino acids 463–476 (red) and 501–514 (orange) in the dimer block the catalytic site. These regions move away from the catalytic site in the tetramer. (*b*) The catalytic site in the SAMHD1 dimer is blocked by the C-terminal region (surface representation). The dNTP substrate cannot gain access to the catalytic site. An artificial dNTP is docked into it and is shown in ball-and-stick representation. (*c*) The C-terminal region moves away from the catalytic site in the tetramer, allowing the dNTP substrate to gain access to the catalytic site.

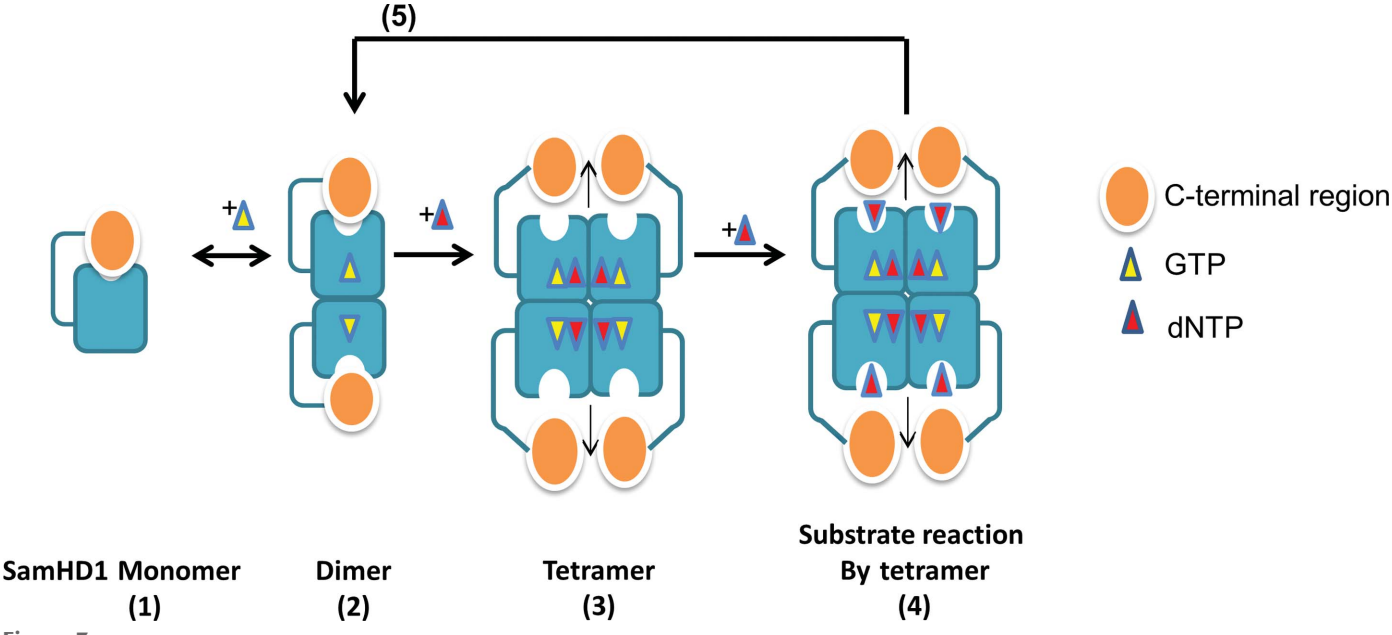

Figure 7
Proposed model for the GTP activation of SAMHD1 dNTPase activity. The SAMHD1 monomer (1) forms a dimer when GTP binds to the G site in the allosteric pocket (2). The C-terminal region of SAMHD1 blocks the catalytic site. In the presence of a high concentration of dNTPs, SAMHD1 forms an activated tetramer after dNTP binds to the S site in the allosteric pocket (3). This binding induces conformational changes in SAMHD1 that allow the C-terminal region to move away from the catalytic site. Substrates enter the catalytic sites and trigger the enzymatic reaction (4). When the substrate concentration drops below a certain level, the tetrameric SAMHD1 disassociates into the inactive dimeric form (5).

mutants isolated from disease patients are defective in dNTPase activity. Our studies lay the foundation for further basic biological research into how SAMHD1 functions in immune tolerance, cancer development, resting-cell survival and restriction of pathogens.

Acknowledgements

We thank Drs Haoran Guo, Sean Evans, Xianjun Liu and Mei Li for technical assistance, Sean Prigge, Wei Xie, Wei Qi and Xiaohong Qin for thoughtful discussions and Deborah McClellan for editorial assistance. We also thank the staff and management of Photon Factory (Japan) beamline BL17A and Shanghai Synchrotron Radiation Facility beamline BL17U for assistance with data collection. This work was supported in part by funding from the Chinese Ministry of Science and Technology (grant Nos. 2012CB911100, 2012CB911103 and 2013ZX0001-005) and the Chinese Ministry of Education (grant No. IRT1016), the Key Laboratory of Molecular Virology, Jilin Province (grant No. 20102209), China, the National Natural Science Foundation of China (grant No. 31270791), the Innovation Foundation of IHEP and Tianjin University.

References

Accola, M. A., Bukovsky, A. A., Jones, M. S. & Göttlinger, H. G. (1999). *J. Virol.* **73**, 9992–9999.
Adams, P. D. *et al.* (2010). *Acta Cryst.* D**66**, 213–221.
Ahn, J., Hao, C., Yan, J., DeLucia, M., Mehrens, J., Wang, C., Gronenborn, A. M. & Skowronski, J. (2012). *J. Biol. Chem.* **287**, 12550–12558.
Amie, S. M., Bambara, R. A. & Kim, B. (2013). *J. Biol. Chem.* **288**, 25001–25006.
Ayinde, D., Casartelli, N. & Schwartz, O. (2012). *Nature Rev. Microbiol.* **10**, 675–680.
Baldauf, H. M. *et al.* (2012). *Nature Med.* **18**, 1682–1687.
Berger, A. *et al.* (2011). *PLoS Pathog.* **7**, e1002425.
Berger, G., Turpin, J., Cordeil, S., Tartour, K., Nguyen, X.-N., Mahieux, R. & Cimarelli, A. (2012). *J. Biol. Chem.* **287**, 41210–41217.
Brandariz-Nuñez, A., Valle-Casuso, J. C., White, T. E., Laguette, N., Benkirane, M., Brojatsch, J. & Diaz-Griffero, F. (2012). *Retrovirology*, **9**, 49.
Clifford, R. *et al.* (2014). *Blood*, **123**, 1021–1031.
Descours, B., Cribier, A., Chable-Bessia, C., Ayinde, D., Rice, G., Crow, Y., Yatim, A., Schwartz, O., Laguette, N. & Benkirane, M. (2012). *Retrovirology*, **9**, 87.
Emsley, P. & Cowtan, K. (2004). *Acta Cryst.* D**60**, 2126–2132.
Engh, R. A. & Huber, R. (1991). *Acta Cryst.* A**47**, 392–400.
Franzolin, E., Pontarin, G., Rampazzo, C., Miazzi, C., Ferraro, P., Palumbo, E., Reichard, P. & Bianchi, V. (2013). *Proc. Natl Acad. Sci. USA*, **110**, 14272–14277.
Gavegnano, C., Kennedy, E. M., Kim, B. & Schinazi, R. F. (2012). *Mol. Biol. Int.* **2012**, 625983.
Goldstone, D. C., Ennis-Adeniran, V., Hedden, J. J., Groom, H. C., Rice, G. I., Christodoulou, E., Walker, P. A., Kelly, G., Haire, L. F., Yap, M. W., de Carvalho, L. P., Stoye, J. P., Crow, Y. J., Taylor, I. A. & Webb, M. (2011). *Nature (London)*, **480**, 379–382.
Hansen, E. C., Seamon, K. J., Cravens, S. L. & Stivers, J. T. (2014). *Proc. Natl Acad. Sci. USA*, **111**, E1843–E1851.
Henderson, L. E., Sowder, R. C., Copeland, T. D., Benveniste, R. E. & Oroszlan, S. (1988). *Science*, **241**, 199–201.
Hofmann, H., Logue, E. C., Bloch, N., Daddacha, W., Polsky, S. B., Schultz, M. L., Kim, B. & Landau, N. R. (2012). *J. Virol.* **86**, 12552–12560.
Hollenbaugh, J. A., Gee, P., Baker, J., Daly, M. B., Amie, S. M., Tate, J., Kasai, N., Kanemura, Y., Kim, D.-H., Ward, B. M., Koyanagi, Y. & Kim, B. (2013). *PLoS Pathog.* **9**, e1003481.
Hrecka, K., Hao, C., Gierszewska, M., Swanson, S. K., Kesik-Brodacka, M., Srivastava, S., Florens, L., Washburn, M. P. & Skowronski, J. (2011). *Nature (London)*, **474**, 658–661.
Ji, X., Tang, C., Zhao, Q., Wang, W. & Xiong, Y. (2014). *Proc. Natl Acad. Sci. USA*, **111**, E4305–E4314.
Ji, X., Wu, Y., Yan, J., Mehrens, J., Yang, H., DeLucia, M., Hao, C., Gronenborn, A. M., Skowronski, J., Ahn, J. & Xiong, Y. (2013). *Nature Struct. Mol. Biol.* **20**, 1304–1309.
Kim, E. T., White, T. E., Brandariz-Núñez, A., Diaz-Griffero, F. & Weitzman, M. D. (2013). *J. Virol.* **87**, 12949–12956.
Laguette, N., Sobhian, B., Casartelli, N., Ringeard, M., Chable-Bessia, C., Ségéral, E., Yatim, A., Emiliani, S., Schwartz, O. & Benkirane, M. (2011). *Nature (London)*, **474**, 654–657.
Lahouassa, H. *et al.* (2012). *Nature Immunol.* **13**, 223–228.
Landau, D. A. *et al.* (2013). *Cell*, **152**, 714–726.
Laskowski, R. A., MacArthur, M. W., Moss, D. S. & Thornton, J. M. (1993). *J. Appl. Cryst.* **26**, 283–291.
Murshudov, G. N., Skubák, P., Lebedev, A. A., Pannu, N. S., Steiner, R. A., Nicholls, R. A., Winn, M. D., Long, F. & Vagin, A. A. (2011). *Acta Cryst.* D**67**, 355–367.
Otwinowski, Z. & Minor, W. (1997). *Methods Enzymol.* **276**, 307–326.
Paxton, W., Connor, R. I. & Landau, N. R. (1993). *J. Virol.* **67**, 7229–7237.
Powell, R. D., Holland, P. J., Hollis, T. & Perrino, F. W. (2011). *J. Biol. Chem.* **286**, 43596–43600.
Rice, G. I. *et al.* (2009). *Nature Genet.* **41**, 829–832.
Roesch, F. & Schwartz, O. (2013). *EMBO J.* **32**, 2427–2429.
Schwefel, D., Groom, H. C., Boucherit, V. C., Christodoulou, E., Walker, P. A., Stoye, J. P., Bishop, K. N. & Taylor, I. A. (2014). *Nature (London)*, **505**, 234–238.
Selig, L., Pages, J.-C., Tanchou, V., Prévéral, S., Berlioz-Torrent, C., Liu, L. X., Erdtmann, L., Darlix, J.-L., Benarous, R. & Benichou, S. (1999). *J. Virol.* **73**, 592–600.
Vagin, A. & Teplyakov, A. (2010). *Acta Cryst.* D**66**, 22–25.
Wei, W., Guo, H., Han, X., Liu, X., Zhou, X., Zhang, W. & Yu, X.-F. (2012). *Cell. Microbiol.* **14**, 1745–1756.
Winn, M. D. *et al.* (2011). *Acta Cryst.* D**67**, 235–242.
Wu, X., Conway, J. A., Kim, J. & Kappes, J. C. (1994). *J. Virol.* **68**, 6161–6169.
Yan, J., Kaur, S., DeLucia, M., Hao, C., Mehrens, J., Wang, C., Golczak, M., Palczewski, K., Gronenborn, A. M., Ahn, J. & Skowronski, J. (2013). *J. Biol. Chem.* **288**, 10406–10417.
Yu, X.-F., Ito, S., Essex, M. & Lee, T.-H. (1988). *Nature (London)*, **335**, 262–265.
Yu, X.-F., Yu, Q.-C., Essex, M. & Lee, T.-H. (1991). *J. Virol.* **65**, 5088–5091.
Zhao, K., Du, J., Han, X., Goodier, J. L., Li, P., Zhou, X., Wei, W., Evans, S. L., Li, L., Zhang, W., Cheung, L. E., Wang, G., Kazazian, H. H. Jr & Yu, X.-F. (2013). *Cell. Rep.* **4**, 1108–1115.
Zhu, C., Gao, W., Zhao, K., Qin, X., Zhang, Y., Peng, X., Zhang, L., Dong, Y., Zhang, W., Li, P., Wei, W., Gong, Y. & Yu, X.-F. (2013). *Nat.ure Commun.* **4**, 2722.